New results on protons inside the South Atlantic Anomaly, at energies between 40 and 250 MeV in the period 2018–2020, from the CSES-01 satellite mission

Matteo Martucci,[1,2] Simona Bartocci,[1] Roberto Battiston,[3,4,*] William Jerome Burger,[4,14] Donatella Campana,[5] Luca Carfora,[1,2] Livio Conti,[1,7] Andrea Contin,[8,9] Cinzia De Donato,[1] Cristian De Santis,[1] Francesco Maria Follega,[3,4] Roberto Iuppa,[3,4] Nadir Marcelli,[1,2] Giuseppe Masciantonio,[1] Matteo Mergè,[1,†] Alberto Oliva,[9] Giuseppe Osteria,[5] Francesco Palma,[1,†] Alexandra Parmentier,[10] Francesco Perfetto,[5] Piergiorgio Picozza,[1,2] Michele Pozzato,[9] Ester Ricci,[3,4] Marco Ricci,[11] Sergio Bruno Ricciarini,[6] Zouleikha Sahnoun,[9] Valentina Scotti,[5,12] Alessandro Sotgiu,[1,2] Roberta Sparvoli,[1,2] Vincenzo Vitale,[1] Simona Zoffoli,[13] and Paolo Zuccon[3,4]

(CSES/Limadou Collaboration)

[1]*INFN-Sezione di Roma "Tor Vergata", V. della Ricerca Scientifica 1, I-00133 Rome, Italy*
[2]*University of Rome "Tor Vergata", V. della Ricerca Scientifica 1, I-00133 Rome, Italy*
[3]*University of Trento, V. Sommarive 14, I-38123 Povo (Trento), Italy*
[4]*INFN-TIFPA, V. Sommarive 14, I-38123 Povo (Trento), Italy*
[5]*INFN-Sezione di Napoli, V. Cintia, I-80126 Naples, Italy*
[6]*IFAC-CNR, V. Madonna del Piano 10, I-50019 Sesto Fiorentino (Florence), Italy*
[7]*Uninettuno University, C.so V. Emanuele II 39, I-00186 Rome, Italy*
[8]*University of Bologna, V.le C. Berti Pichat 6/2, I-40127 Bologna, Italy*
[9]*INFN-Sezione di Bologna, V.le C. Berti Pichat 6/2, I-40127 Bologna, Italy*
[10]*INAF-IAPS, V. Fosso del Cavaliere 100, I-00133 Rome, Italy*
[11]*INFN-LNF, V. E. Fermi 54, I-00044 Frascati (Rome), Italy*
[12]*University of Naples "Federico II", V. Cintia 21, I-80126 Naples, Italy*
[13]*Italian Space Agency, V. del Politecnico, I-00133 Rome, Italy*
[14]*Centro Fermi, V. Panisperna 89a, I-00184 Rome, Italy*

(Received 9 June 2021; accepted 14 January 2022; published 18 March 2022; corrected 29 March 2022 and 7 July 2022)

The High-Energy Particle Detector (HEPD) on board the China Seismo-Electromagnetic Satellite (CSES-01) was launched in February 2018, with a foreseen mission lifetime of over 5 years. It is providing crucial new insight in the physical dynamics of the radiation belts in the Earth's magnetosphere, in particular in the South Atlantic Anomaly (SAA). In this work, proton data from HEPD in the 40 MeV–250 MeV energy range, collected inside the SAA during the period between August 2018 and December 2020, are presented and compared with the up-to-date AP9 model by NASA. These are the first results on SAA protons at Low-Earth Orbit during the minimum activity phase between the 24th and the 25th solar cycles below 250 MeV. They enable an extensive testing and validation of current theoretical and empirical models aimed at predictions of temporal changes in this critical region of space. HEPD is advancing the observations collected by the PAMELA space experiment and NASA Van Allen Probe during the last 15 years through the 23rd and 24th solar cycles.

DOI: 10.1103/PhysRevD.105.062001

I. EARTH'S RADIATION BELTS AND SOUTH ATLANTIC ANOMALY

Galactic proton cosmic rays above ~1 GeV are considered as the main source of the cosmic ray albedo neutron decay (CRAND) mechanism [1,2]; they interact with the neutral molecules in the upper atmosphere, generating energetic albedo neutrons which decay into protons (along with electrons and antineutrinos). Such protons are trapped by the Earth's magnetic field, contributing to the so-called inner radiation belt [3]. The region where the inner belt comes closest to the Earth's surface—approximately located over the South Atlantic Ocean—is known as the South Atlantic Anomaly (SAA). The SAA emerges as a consequence of the tilt (~10°) between the magnetic dipole axis of the Earth and its rotational axis, and of the offset (~500 km) between the dipole itself and the Earth's center [4]. It is characterized by

*roberto.battiston@unitn.it
†Also at ASI Space Science Data Center (SSDC), V. del Politecnico, I-00133 Rome, Italy.

an extremely low intensity of the geomagnetic field, which shows a certain level of variability over time [5,6]. Several studies show that the extent of the SAA has been continuously growing since its discovery [7] and that the magnetic dipole strength has been decreasing [8]. This phenomenon has been related to a possible upcoming reversal or excursion of the geomagnetic field, which could heavily affect human activities on Earth and in space [9–11]. In addition, it is well known that the radiation belts in the Earth's magnetosphere pose a hazard to human spaceflights and satellite systems, massively affecting design and resources for spacecraft and payloads. For this reason, the scientific community has been considerably involved in modeling the space radiation environment [12,13]. The NASA AE9/AP9 set of models for electrons and protons, respectively, is the most recent effort in describing the near Earth radiation environment. These models are based on numerous datasets, obtained from sensors on board various satellites and processed to create maps of the particle fluxes with different estimated uncertainties, from both dedicated and not-dedicated missions and from space weather variability [13,14]. However, such models are incomplete since their predictions are not based on a statistically sufficient sample of direct measurements [15]. Consequently, reliable sets of data from in-flight instruments, covering long periods of time, are crucial to improve their output and accuracy. The High-Energy Particle Detector (HEPD), orbiting on board the China Seismo-Electromagnetic Satellite CSES-01, with a foreseen lifetime of 5+ years, is now providing precise data that enables testing and validation of the aforementioned models [13].

II. CSES/LIMADOU MISSION AND HIGH-ENERGY PARTICLE DETECTOR

The CSES-01 satellite [16] was launched on February 2, 2018, and is currently flying on a sun-synchronous polar orbit at a ∼507 km altitude, with a 5-day revisiting periodicity. It is the first of a series of multi-instrument satellites, scheduled for launch in a few years, mainly dedicated to the monitoring of electromagnetic field, plasma and particle perturbations in the ionosphere and magnetosphere, due to natural sources like earthquakes or artificial emitters. The tracking of solar modulation and of Van Allen belt modifications in time, are other very important scientific objectives. The orbital characteristics, together with the fact that payloads on board the satellite are switched off at latitudes below −65° and above +65°, do not allow a detailed investigation of the outer belts, but they do allow an extensive study of the inner belt, in particular of the South Atlantic Anomaly. HEPD is one of the nine instruments on board the satellite. It has been designed and built in the framework of the CSES/Limadou project by the Italian branch of the CSES Italian-Chinese Collaboration. It is a light and compact payload (40.36 cm× 53.00 cm × 38.15 cm, total mass ∼45 kg), made up of a series of subdetectors; from the top of the detector, two double-sided silicon microstrips planes (213.2 mm× 214.8 mm × 0.3 mm) providing a tracking system, a layer of plastic segmented scintillator (6 paddles, 20 cm × 3 cm × 0.5 cm each), a range calorimeter for energy measurement composed of a stack (TOWER) of 16 plastic scintillators [$P_1 \ldots P_{16}$ (15 cm × 15 cm × 1 cm)], and a 3 × 3 matrix of lutetium-yttrium oxyorthosilicate inorganic scintillator crystals (5 cm × 5 cm × 4 cm). The instrument is surrounded—laterally and at the bottom—by five plastic scintillators which reject particles that do not deposit all their energy inside the detector (VETO). The trigger comprises the stripped scintillator, to recognize multiple events, and the first and second plane of the calorimeter. The detector is optimized to measure electrons in the 3 MeV to 100 MeV energy range, and protons between 40 MeV and 250 MeV, as well as light nuclei. The HEPD capabilities for protons have already been assessed in [17], while more technical details on the instrument can be found in [18,19].

III. DATA ANALYSIS

Electrons, protons, and light nuclei were distinguished by the usual ΔE vs E method, with ΔE provided by the analog-to-digital converter (ADC) signal deposited on the P_1 scintillator plane—converted to deposited energy thanks to extensive Monte Carlo simulations with digitization and E the total energy released in the calorimeter. Inside the SAA, the trapped electrons are mainly confined to energies lower than 8 MeV [20], thus not affecting the 40 MeV–250 MeV energy range for protons analyzed in this work. Contamination from antiprotons is negligible [21], and no attempt was made to discriminate between pseudo-trapped, quasitrapped, and precipitating protons, which account for less than 10% of the trapped population [22]. The aforementioned ADC signal distribution of protons on plane P_1 as a function of the total energy lost in the calorimeter is shown in Fig. 1. As can be seen, no electron population appears above 50 MeV in the plot; more information on the particle identification capabilities of the HEPD instrument can be found in [17–19].

The overall acceptance of the detector is defined by the requirement of containment within the volume of the instrument, i.e., an incoming particle, entering the upmost section of the payload, must be fully contained inside the calorimeter to collect all its energy. It is evaluated using a GEANT4-based Monte Carlo simulation of isotropically generated ($0° < \theta < 90°$ and $0° < \phi < 180°$, where θ and ϕ are the zenith and azimuth angles, respectively) protons with primary energy ranging from 10 MeV to 400 MeV. The acceptance shows a strong energy dependence, with a maximum value of ∼400 cm^2 sr at ∼90 MeV, steeply decreasing, at lower energies due to energy losses, and at higher energies due to the higher penetration power and production of secondaries that may hit one or more

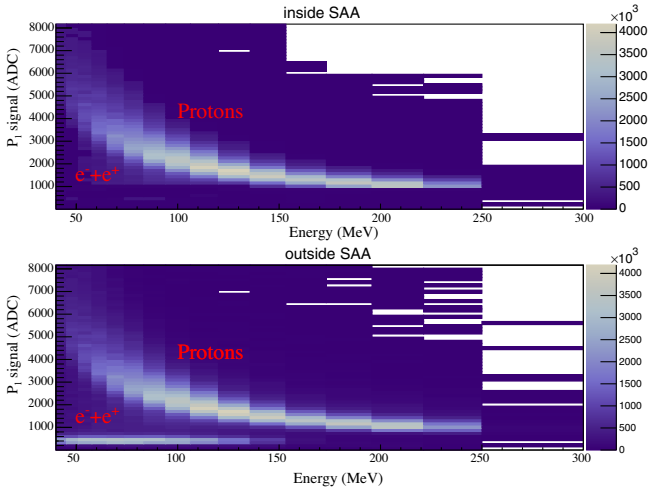

FIG. 1. Vertical ($\theta < 15°$) proton electronics ADC signal on plane P_1 as a function of the total energy deposited in the calorimeter inside (top panel) and outside the SAA (bottom panel). The absence of any electron population inside the Anomaly—which would have been confined in the area around 500 ADC—is evident.

VETO planes [17,18]. As stated before, the absence of trapped electrons/positrons above 50 MeV allows a contamination-free analysis, so no selection was used to discriminate protons from other lepton populations. The only efficiency entering this analysis is the trigger efficiency, which was estimated to be ∼95%. The SAA region, where the proton sample of this work was collected, has been defined by a magnetic field lower than 20500 nT (calculated using the IGRF-12 routines [8]) and McIlwain parameter [23] L-shell < 1.3 (calculated using the IRBEM libraries [24]). The live time $\tau_{\rm live}$ of the instrument was managed via the acquisition system, as described in [25]. Even though the particle rate inside the SAA is the highest registered along the CSES orbit, no major saturation issue was detected for > 40 MeV protons. Due to the extreme anisotropy of proton population inside the Anomaly, the flux estimation has been performed using a multidimensional matrix approach, following the methods described in [26,27]. Therefore, final directional differential fluxes $F(\chi, E, \alpha)$ were obtained using the following equation,

$$F(\chi, E, \alpha) = \frac{N(\chi, E, \alpha)}{2\pi H(\Psi, E, \alpha)\Delta\tau(\Psi)\Delta E\Delta\alpha}, \qquad (1)$$

where $N(\chi, E, \alpha)$ is the number of proton candidates as a function of the position χ = (longitude, latitude), energy E and local pitch angle α—i.e., the angle between the particle's velocity vector and local magnetic field—and $\Delta\tau(\Psi)$ is the live time spent by the satellite at each spacecraft orientation Ψ, while the effective area of the instrument, $H(\Psi, E, \alpha)$, is defined as

$$H(\Psi, E, \alpha) = \frac{\sin\alpha}{2\pi}\int_0^{2\pi} d\beta A(E, \theta, \phi)\cos\theta, \qquad (2)$$

where β is the gyrophase angle and $A(E, \theta, \phi)$ is the directional-dependent response function of the apparatus with θ,ϕ the orientation angles. To have enough statistics, a bin size of 5° for longitude, 3° for latitude, 30° for both θ and ϕ, and 5° for the local pitch angle, was chosen. A total of 14 logarithmic energy bins were used to estimate proton spectra. An unfolding procedure, following the classical Bayesian approach proposed in [28,29], was employed to correct for particle slow-down and energy loss in the passive structures and energy loss due to inelastic interactions. A more detailed description of the procedure is reported in [17].

IV. RESULTS

HEPD fluxes, averaged over the entire period 2018–2020, are shown in Fig. 2, compared to the predictions of the NASA AP9 empirical model [14]. The NASA model provides estimates of uncertainties from both dedicated and nondedicated missions and space weather variability, obtained as statistical confidence levels; for example, in this analysis the 95% C.L. is used. On the other hand, errors on HEPD data account for both statistical and systematic uncertainties. Possible sources of systematics lie in the deconvolution procedure and the comparison between data and Monte Carlo; the former is related to the intrinsic accuracy of the adopted unfolding technique, while the latter includes the differences between flight data and Monte Carlo due to the digitization procedure and the limited statistics of the simulated sample. Overall, these uncertainties range between ∼4% and ∼13%, as discussed in [17].

These are the first results on SAA protons at Low-Earth Orbit during the minimum activity phase between the 24th and the 25th solar cycle in the energy range lower than 250 MeV. In the top panel, South Atlantic Anomaly proton spectra over the entire explored energy range and for three different local pitch angle intervals are shown. These are in good agreement with AP9 predictions, except for the 87.5°–92.5° local pitch angle, where they are overestimated. In the middle panel, local pitch angle dependencies for three different energy intervals are presented. There is a good agreement between data and model, except for the higher energy interval. A similar behavior can be observed in the bottom panel of Fig. 2 where the data are plotted as a function of three L-shell intervals, integrated over the whole solid angle. The remarkable stability of the HEPD instrument in measuring particles over time has also allowed for a high-precision and good time-resolution measure of flux intensity variations for omnidirectional protons inside the SAA for the same period and with normalization to the month of August 2018, as reported in Fig. 3.

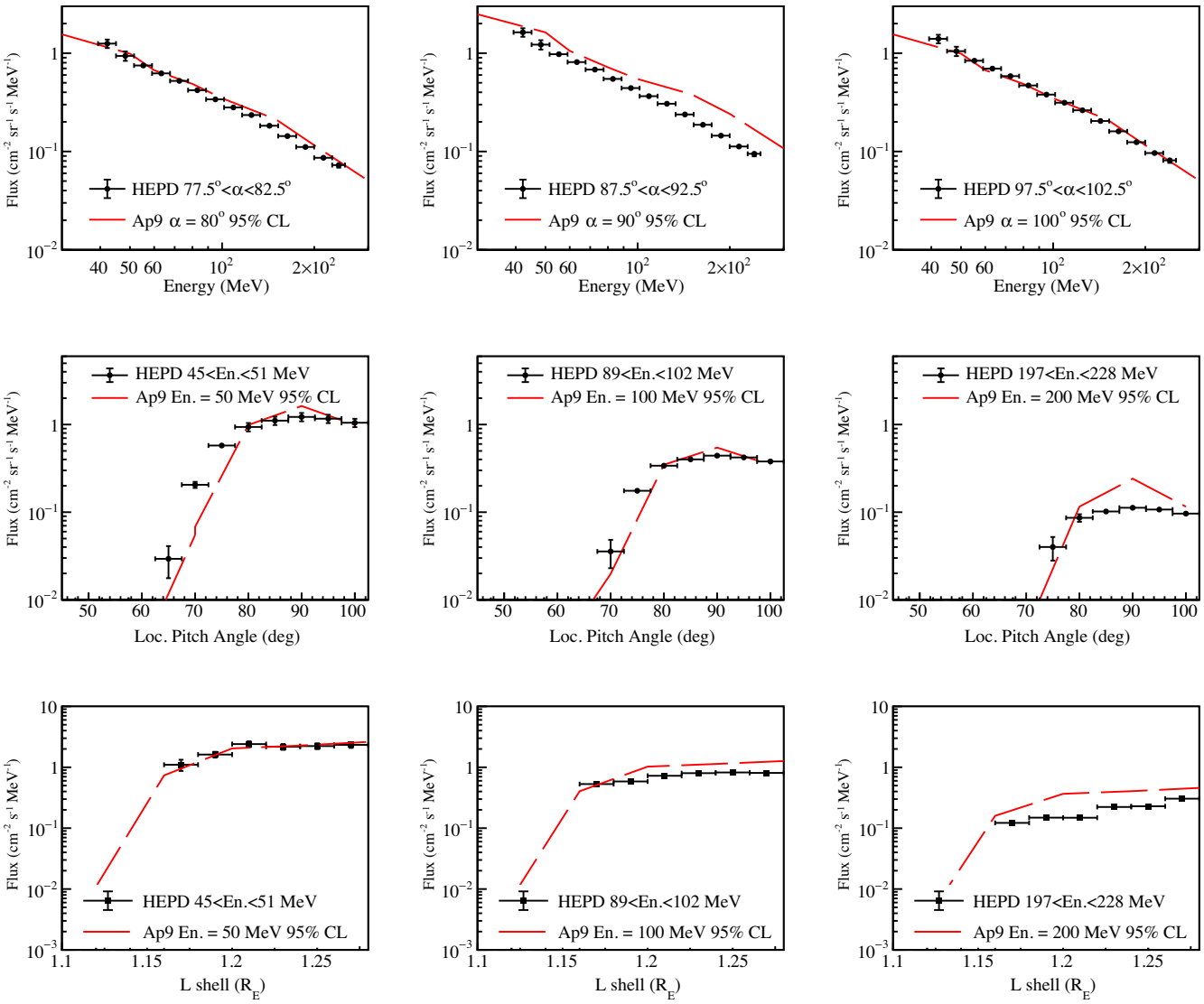

FIG. 2. South Atlantic Anomaly proton fluxes as a function of energy (top panels), local pitch angle (middle panels) and L-shell (Earth radii, bottom panels) obtained by HEPD (black squares) between August 2018 and December 2020, and compared with predictions from the AP9 model at 95% C.L. (red dashed line).

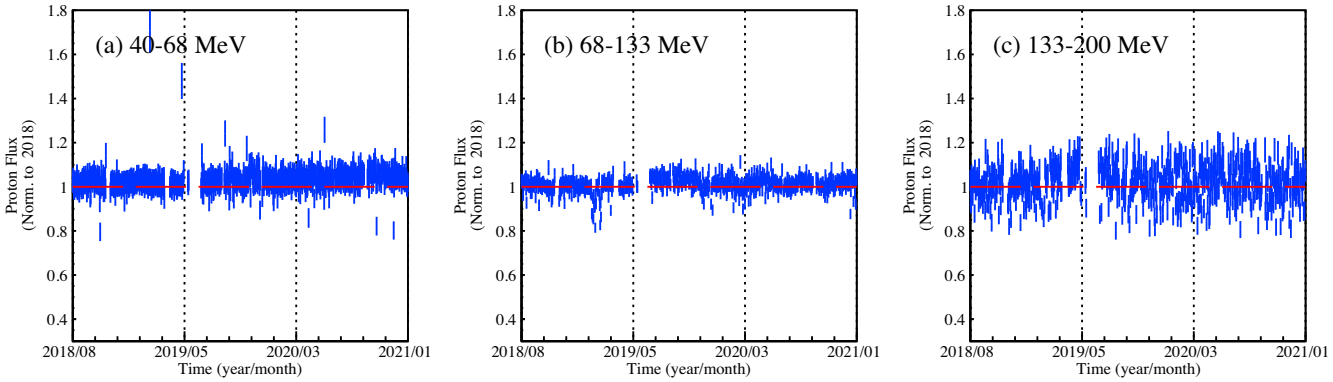

FIG. 3. Time profiles (1-day time binning) of omnidirectional protons inside the SAA measured by HEPD from August 2018 to December 2020, normalized to the month of August 2018. The three panels refer to three different energy ranges; low (40 MeV–68 MeV, left panel), medium (68 MeV–133 MeV, middle panel) and high (133 MeV–200 MeV, right panel). The gap in proton data between May 2019 and June 2019 refers to a period of instrument malfunctioning.

The three panels in Figure 3 refer to three different energy ranges, low (40 MeV–68 MeV, left panel), medium (68 MeV–133 MeV, middle panel) and high (133 MeV–200 MeV, right panel), and show a general constancy of the proton intensity within the SAA region in the period of data collection, taking into account the overall systematic uncertainties. During this time window, only one strong geomagnetic storm occurred on August 25th, 2018 [30] but no evident signatures were observed in energetic protons. This stability is plausibly related to minimal solar activity over the period between mid 2018 and late 2020, with a number of sunspots close to zero. In fact, the variation in the rate of generation of the trapped particle population is linked to the variation in the intensity of the cosmic ray flux entering the heliosphere. Finally, in Fig. 4, geographical maps of the measured omnidirectional proton fluxes in the same period are shown as a function of latitude and longitude for an interval between 40 MeV and 45 MeV (top panel) and between 200 MeV and 230 MeV (bottom panel). In the top panel, it appears that low-energy protons are present in almost the entire region of the SAA, peaking in its central part (bulk). On the contrary, the high-energy protons shown in the bottom panel are more concentrated in the bulk, while they seem practically absent in the peripheral sectors. This is consistent with what was observed in [27]. In both panels, the isolines of the reconstructed magnetic field are also shown for clarity.

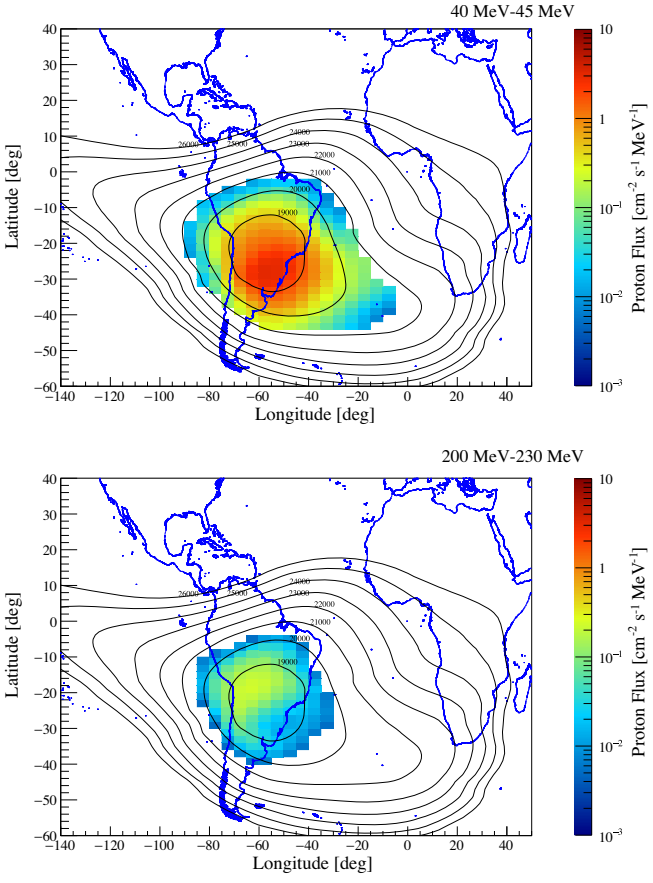

FIG. 4. Geographical maps of omnidirectional proton fluxes (August 2018–December 2020) as a function of latitude and longitude for a low-energy bin (40 MeV–45 MeV, upper panel) and for a higher one (200 MeV–230 MeV, bottom panel). In both panels, the isolines of the reconstructed magnetic field are also shown for clarity.

V. DISCUSSION AND CONCLUSIONS

In this work, new results are presented on protons inside the South Atlantic Anomaly in the energy range 40 MeV–250 MeV, measured by the HEPD on board CSES-01 between August 2018 and December 2020. The remarkable stability of the instrument in the particle measurement and the absence of trapped electrons with energies higher than 8 MeV in the explored region have allowed an almost contamination-free analysis. The very good identification of proton population by the detector and the precise measurements in energy, as well as the application of the multidimensional matrix approach reported in [26], have enabled a correct estimation of the proton flux anisotropy inside the SAA region. The data are in generally good agreement with the AP9 model at 95% C.L., as a function of energy, local pitch angle, and L-shell. Major discrepancies with the model are expected at higher energies, see the second panel in the first row of Fig. 2, where fewer experiments provided valid data to construct good estimates of the fluxes. The PAMELA mission measured trapped protons up to ∼2 GeV [27] in low Earth orbit but these data have not been included in the AP9 model yet. Moreover, the time-intensity profiles of the proton fluxes in three different energy ranges appear to be constant in time, as foreseen for the phase of the solar cycle in which the data have been collected. Finally, the geographical maps of the measured omnidirectional proton fluxes show that the low-energy protons are present in almost the whole SAA region, while the high-energy ones are concentrated in the innermost area, as expected. In conclusion, the HEPD instrument has proven suitable to provide, even for the next years of operation, an excellent cross-calibration for radiation environment models in low Earth orbit, such as the NASA AP9, task performed until October 2019 by the Van Allen Probe missions [31]. HEPD low-energy proton data complement existing measurements obtained by satellites that flew in the SAA region between the 1960s and the 2000s (already inserted in the AP9 model) and also continue the precise analysis of the trapped proton population performed by experiments like PAMELA, adding an evaluation of the proton fluxes in a period of maximum solar activity. With both a good energy and angular resolution, HEPD is able to measure protons inside the SAA with better precision and a higher statistics with respect to the majority of the previous missions included in the AP9 model (thanks to a wide field-of-view), scanning even the

spatial anisotropy of trapped radiation inside the region with high accuracy. Furthermore, the measurement of the trapped components inside the inner Van Allen belt—which is linked to the interaction of primary cosmic rays with the atmosphere via the CRAND mechanism—could be helpful for experiments that are currently studying the properties of high-energy cosmic rays and their variation over time, like AMS-02 [32,33]. In fact, the presence of a direct correlation between solar modulation of such high-energy cosmic protons and changes in trapped populations inside the SAA is yet to be fully understood [34,35]. It is also important to note that HEPD will be followed by HEPD-02 (now under construction) scheduled to be launched at the end of 2022 on board the CSES-02 Chinese satellite, extending the mission through the current decade.

ACKNOWLEDGMENTS

This work makes use of data from the CSES mission [36], a project funded by China National Space Administration (CNSA), China Earthquake Administration (CEA) in collaboration with the Italian Space Agency (ASI), National Institute for Nuclear Physics (INFN), Institute for Applied Physics (IFAC-CNR), and Institute for Space Astrophysics and Planetology (INAF-IAPS). We kindly acknowledge the AFRL for providing the AE9/Ap9/SPM set of models. This work was supported by the Italian Space Agency in the framework of the "Accordo Attuativo 2020-32.HH.0 Limadou Scienza+" (CUP F19C20000110005) and the ASI-INFN Agreement No. n.2014-037-R.0, addendum 2014-037-R-1-2017.

[1] S. F. Singer, Trapped Albedo Theory of the Radiation Belt, Phys. Rev. Lett. **1**, 181 (1958).
[2] T. A. Farley and M. Walt, Source and loss processes of protons of the inner radiation belt, J. Geophys. Res. **76**, 8223 (1971).
[3] J. A. van Allen and L. A. Frank, Radiation measurements to 658,300 Km. with Pioneer IV, Nature (London) **184**, 219 (1959).
[4] J. R. Heirtzler, The future of the south atlantic anomaly and implications for radiation damage in space, J. Atmos. Sol. Terr. Phys. **64**, 1701 (2002).
[5] D. Gubbins, A. L. Jones, and C. C. Finlay, Fall in earth's magnetic field is erratic, Science **312**, 900 (2006).
[6] J. Aubert, Geomagnetic forecasts driven by thermal wind dynamics in the earth's core, Geophys. Suppl. Mon. Not. R. Astron. Soc. **203**, 1738 (2015).
[7] C. F. Gauß, Anzeige der Abhandlung des Herrn Hofr. Gauß: Intensitas vis magneticae terrestris admensuram absolutam revocata, Astron. Nachr. **10**, 349 (1833).
[8] T. Erwan, C. Finlay, C. Beggan, P. Alken, J. Aubert, O. Barrois, F. Bertrand, T. Bondar, A. Boness, L. Brocco, E. D. Canet, A. Chambodut, A. Chulliat, P. Coïsson, F. Civet, A. Du, A. Fournier, I. Fratter, N. Gillet, and T. Zvereva, International geomagnetic reference field: The 12th generation, Earth Planets Space **67**, 79 (2015).
[9] J. Aubert, J. Aurnou, and J. Wicht, The magnetic structure of convection-driven numerical dynamos, Geophys. J. Int. **172**, 945 (2008).
[10] J. Wicht and U. R. Christensen, Torsional oscillations in dynamo simulations, Geophys. J. Int. **181**, 1367 (2010).
[11] A. De Santis, E. Qamili, and L. Wu, Toward a possible next geomagnetic transition?, Nat. Hazards Earth Syst. Sci. **13**, 3395 (2013).
[12] S. Deme, G. Reitz, I. Apáthy, I. Héjja, E. Láng, and I. Fehér, Doses due to the South Atlantic Anomoly during the Euromir'95 mission measured by an on-board TLD system, Radiation Protection Dosimetry **85**, 301 (1999).
[13] M. Martucci *et al.*, Trapped proton fluxes estimation inside the south atlantic anomaly using the nasa ae9/ap9/spm radiation models along the china seismo-electromagnetic satellite orbit, Appl. Sci. **11**, 3465 (2021).
[14] G. P. Ginet, T. P. O'Brien, S. L. Huston, W. R. Johnston, T. B. Guild, R. Friedel, C. D. Lindstrom, C. J. Roth, P. Whelan, R. A. Quinn, D. Madden, S. Morley, and Yi-Jiun Su, AE9, AP9 and SPM: New models for specifying the trapped energetic particle and space plasma environment, Space Sci. Rev. **179**, 579 (2013).
[15] J. Ripa, G. Dilillo, R. Campana, and G. Galgoczi, A comparison of trapped particle models in low earth orbit, Proc. SPIE **11444**, 114443P (2020).
[16] X. H. Shen, X. M. Zhang, S. G. Yuan, L. W. Wang, J. B. Cao, J. P. Huang, X. H. Zhu, P. Picozza, and J. P. Dai, The state-of-the-art of the China Seismo-Electromagnetic Satellite mission, Sci. China E **61**, 634 (2018).
[17] S. Bartocci *et al.*, Galactic cosmic-ray hydrogen spectra in the 40–250 MeV range measured by the High-Energy Particle Detector (HEPD) on board the CSES-01 satellite between 2018 and 2020, Astrophys. J. **901**, 8 (2020).
[18] P. Picozza *et al.*, Scientific goals and in-orbit performance of the High-Energy Particle Detector on board the CSES, Astrophys. J. Suppl. Ser. **243**, 16 (2019).
[19] G. Ambrosi *et al.*, Beam test calibrations of the HEPD detector on board the China Seismo-Electromagnetic Satellite, Nucl. Instrum. Methods Phys. Res., Sect. A **974**, 164170 (2020).
[20] J. F. Fennell, S. G. Claudepierre, J. B. Blake, T. P. O'Brien, J. H. Clemmons, D. N. Baker, H. E. Spence, and G. D. Reeves, Van allen probes show that the inner radiation zone contains no mev electrons: Ect/mageis data, Geophys. Res. Lett. **42**, 1283 (2015).
[21] O. Adriani *et al.*, The discovery of geomagnetically trapped cosmic-ray antiprotons, Astrophys. J. Lett. **737**, L29 (2011).
[22] O. Adriani *et al.*, Reentrant albedo proton fluxes measured by the PAMELA experiment, J. Geophys. Res. **120**, 3728 (2015).

[23] This parameter describes a particular set of planetary magnetic field lines which cross the Earth's magnetic equator at a number of Earth-radii equal to the parameter value itself.
[24] J. G. Roederer and H. Zhang, *Dynamics of Magnetically Trapped Particles* (Springer-Verlag Berlin Heidelberg, Berlin, 2014), Vol. 403.
[25] G. Ambrosi *et al.*, The electronics of the High-Energy Particle Detector on board the CSES-01 satellite, Nucl. Instrum. Methods Phys. Res., Sect. A **1013**, 165639 (2021).
[26] R. S. Selesnick, A. C. Cummings, J. R. Cummings, R. A. Mewaldt, E. C. Stone, and T. T. von Rosenvinge, Geomagnetically trapped anomalous cosmic rays, J. Geophys. Res. **100**, 9503 (1995).
[27] O. Adriani *et al.*, Trapped proton fluxes at low earth orbits measured by the PAMELA experiment, Astrophys. J. **799**, L4 (2015).
[28] G. D'Agostini, A multidimensional unfolding method based on Bayes' theorem, Nucl. Instrum. Methods Phys. Res., Sect. A **362**, 487 (1995).
[29] G. D'Agostini, Improved iterative Bayesian unfolding, arXiv:1010.0632.
[30] F. Palma *et al.*, The august 2018 geomagnetic storm observed by the High-Energy Particle Detector on board the CSES-01 satellite, Appl. Sci. **11**, 5680 (2021).
[31] J. Mazur, L. Friesen, A. Lin, D. Mabry, N. Katz, Y. Dotan, J. George, J. B. Blake, M. Looper, M. Redding, T. P. O'Brien, J. Cha, A. Birkitt, P. Carranza, M. Lalic, F. Fuentes, R. Galvan, and M. McNab, The relativistic proton spectrometer (RPS) for the radiation belt storm probes mission, Space Sci. Rev. **179**, 221 (2013).
[32] M. Aguilar *et al.*, Observation of Fine Time Structures in the Cosmic Proton and Helium Fluxes with the Alpha Magnetic Spectrometer on the International Space Station, Phys. Rev. Lett. **121**, 051101 (2018).
[33] M. Aguilar *et al.*, The alpha magnetic spectrometer (ams) on the international space station: Part II—results from the first seven years, Phys. Rep. **894**, 1 (2021).
[34] M. A. K. Lodhi, A. B. Diaz, and T. L. Wilson, Simplified solar modulation model of inner trapped belt proton flux as a function of atmospheric density, Radiation Measurements **39**, 391 (2005).
[35] A. Bruno *et al.*, Solar-cycle variations of south atlantic anomaly proton intensities measured with the PAMELA mission, Astrophys. J. Lett. **917**, L21 (2021).
[36] www.leos.ac.cn/.

Correction: The previously published Fig. 4 in the PDF version was processed improperly during the final production cycle and its rendition has been corrected. The title contained minor errors and has been set right.

Second Correction: The name and affiliation of an author were missing in the original publication and have been inserted.